THE JOURNAL OF PHYSICAL CHEMISTRY B

ARTICLE

pubs.acs.org/JPCB

Absorption, Circular Dichroism, and Photoluminescence in Perylene Diimide Bichromophores: Polarization-Dependent H- and J-Aggregate Behavior

K. A. Kistler,[†] C. M. Pochas,[‡] H. Yamagata,[‡] S. Matsika,[‡] and F. C. Spano*[,†]

[†]Department of Chemistry, Pennsylvania State University, Brandywine Campus Media, Pennsylvania 19063, United States

[‡]Department of Chemistry, Temple University, Philadelphia, Pennsylvania 19122, United States

ABSTRACT: Using a single-mode Holstein Hamiltonian with through-space excitonic couplings evaluated quantum mechanically, the absorption, circular dichroism, and photoluminescence spectral line shapes of a chiral perylene diimide dimer complex were accurately reproduced. In general, a dimer consisting of two chromophores related through a C_2 rotation is neither a J- nor an H-aggregate because oscillator strength is divided between the top and bottom of the exciton band. The division gives rise to the two Davydov components per vibronic band in the absorption spectrum. Nevertheless, it is shown that the vibronic structure of the absorption component polarized in the same direction as the lower (upper) Davydov component is identical to what one would obtain from an ideal J- (H-) aggregate. Emission generally contains both polarization components, but the component polarized in the same direction as the lower (upper) Davydov component behaves similarly to the emission from an ideal J- (H-) aggregate. The basic photophysical behavior also applies to molecular crystals containing two molecules per unit cell in which the interactions between inequivalent molecules dominate over interactions between equivalent molecules.

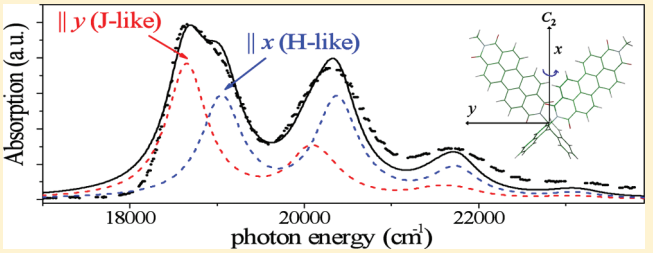

I. INTRODUCTION

The classification of J- versus H-aggregates, developed many decades ago largely through the efforts of Kasha and co-workers,[1−3] was a key development in understanding the relationship between morphology and photophysical function in molecular assemblies. Electronic interactions between molecules induce delocalized excited states, or Frenkel excitons, which are identified through a red shift (blue shift) of the main absorption peak in J- (H-) aggregates compared to isolated molecules in solution. Radiative properties are also affected quite differently in the two aggregate types: In J- (H-) aggregates, the symmetry of the lowest-energy exciton dictates enhanced (depressed) radiative decay rates relative to the monomer.

The aggregation-induced shift in the absorption spectrum is not always a reliable indicator of J- or H-aggregation. In the case of weakly coupled H-aggregates, the excitonic blue shift can easily be dominated by a much larger red shift due to nonresonant interactions[4]—the so-called gas-to-crystal shift. In polymer H-aggregates, the red shift due to the enhanced planarization of the polymers within an aggregate can also dominate the weak blue shift, as happens in poly(3-hexylthiphene) thin films.[5,6] Moreover, J versus H assignments based on radiative decay rates are not straightforward: The radiative decay rate must be disentangled from nonradiative rates, which often requires rather delicate measurements of the temperature-dependent absolute quantum yield.

Fortunately, additional spectral signatures for J- and H-aggregates can be identified from the way vibronic coupling in molecules is altered by intermolecular interactions.[7] In many aggregate-forming dye molecules and π-conjugated molecules in general, the main $S_0 \rightarrow S_n$ electronic transitions are coupled to the symmetric vinyl stretching mode (or cluster of modes) with frequencies near 1400 cm^{-1}, resulting in pronounced vibronic progressions in the absorption and photoluminescence (PL) spectra. In aggregates, additional signatures arise from the opposing manners in which the progression is distorted upon H- or J-aggregation, as outlined in ref 7. Briefly, the ratio of the oscillator strengths of the first two vibronic peaks in the absorption spectrum, I_A^{0-0}/I_A^{1-0}, increases (decreases) in J- (H-) aggregates relative to the monomer. In the PL spectrum, the line strength ratio, $I_{PL}^{0-0}/I_{PL}^{0-1}$, decreases (increases) with increasing temperature and increasing disorder in J- (H-) aggregates. Although these properties are strictly valid in ideal aggregates containing one molecule per unit cell, we show in this article how they are modified when there are two molecules per unit cell. We focus on a simple dimer complex in which the two molecules are related by a C_2 rotation. Our results can be directly applied to the popular herringbone packing lattices adopted by many organic chromophores, where the two molecules in a unit cell are related by a 2-fold screw rotation or glide plane translation.

In this article, we analyze in detail the absorption, circular dichroism (CD), and PL spectra of a chiral perylene diimide (PDI) complex consisting of two PDI chromophores covalently

Received: September 12, 2011
Revised: November 4, 2011
Published: December 15, 2011

bonded through a naphthalene bridge.[8] PDI chromophores have been extensively studied because of their near-unit quantum yields and their ability to readily self-assemble in a variety of geometries leading to both J- and H-aggregates, depending mainly on the attached side groups.[9−11] There has also been significant interest in covalently linked PDI complexes[8,12−17] and PDI/DNA complexes.[18−20] Theoretical analysis of the impact of vibronic coupling on the absorption spectrum of molecular dimers began with the work of Witkowski[21] and Fulton and Gouterman.[22,23] The CD spectrum of dimers was originally treated by Weigang.[24,25] Several recent theoretical works have successfully described many of the salient features of the absorption and emission spectral line shapes of PDI dimers[26−29] and crystals based on perylene derivatives,[30,31] including the effects of vibronic coupling.

For packing arrangements with one molecule per unit cell, the I_A^{0-0}/I_A^{1-0} ratio is primarily determined by the Huang−Rhys (HR) factor corresponding to the vinyl stretching mode and the free exciton bandwidth, W, which measures the strength of the intermolecular couplings. The HR factor is easily obtained from the absorption spectrum of the monomer in solution. Hence, from the measured value of I_A^{0-0}/I_A^{1-0}, one can readily deduce W. This method was successfully applied to determine the exciton bandwidth in polythiophene π-stacks.[5,6]

In packing arrangements with two molecules per unit cell, oscillator strength is generally deposited at the top and bottom of the exciton bands, giving rise to the two Davydov components in the absorption spectrum.[32,33] The two components are polarized differently, and each one yields a separate value for I_A^{0-0}/I_A^{1-0}. As we show herein, the vibronic progression corresponding to the lower-energy Davydov component is identical to that of an ideal J-aggregate, with I_A^{0-0}/I_A^{1-0} increasing with W, whereas the vibronic progression corresponding to the higher-energy Davydov component is identical to that of an ideal H-aggregate, with I_A^{0-0}/I_A^{1-0} decreasing with W. Although measuring the individual polarized components for a PDI complex in solution is not possible because of the isotropic distribution of molecular orientations, in a fixed crystalline lattice, such as the herringbone lattice, it is possible. The PL spectrum for aggregates with two molecules per unit cell generally contains both polarization components: a J-like component in which the 0−0 emission is allowed and an H-like component in which the 0−0 emission is absent (as long as the symmetry is preserved, i.e., there is no disorder). We have recently shown that the ratio of the line strengths of the first two vibronic peaks, $I_{PL}^{0-0}/I_{PL}^{0-1}$, in the J-like component provides a direct measure of the exciton coherence number.[34]

The more conventional way of determining W from the absorption spectrum is directly from the Davydov splitting (DS). However, in packing arrangements with one molecule per unit cell, there is no DS (as one component carries no oscillator strength), making the ratio method a more robust technique for obtaining W. In the PDI bichromophore in the present study, the two PDI molecules are almost at right angles to each other. Hence, this system presents a unique opportunity to evaluate the two methods for obtaining W. We also compare the values of W extracted from the absorption spectrum with the value computed using a novel transition charge density technique.

II. ABSORPTION AND CIRCULAR DICHROISM (CD) IN PDI COMPLEXES

We begin by reviewing the salient features of the absorption and CD spectra of the naphthalene-bridged PDI_2 bichromophore shown in Figure 1. The solution-phase spectra of the PDI monomer (with 1-hexylheptyl end groups) and the PDI_2 complex from ref 8 are reproduced in Figure 2. The spectra derive from the electronic $S_0 \rightarrow S_1$ transition and are characterized by a pronounced vibronic progression due to the vinyl stretching mode with frequency $\hbar\omega_0 \approx 0.17$ eV (1400 cm^{-1}). In the monomer, the vibronic peaks are labeled as $0 \leftarrow 0$, $1 \leftarrow 0$, $2 \leftarrow 0$, and so on (abbreviated as 0−0, 1−0, 2−0, etc.) in order of increasing energy. The monomer absorption spectral line shape is well-described using an expression based on shifted S_0 and S_1 nuclear potential wells of identical curvature,

$$A_{mon}(\omega) = \sum_{n=0,1,2,\ldots} \frac{e^{-\lambda^2}\lambda^{2n}}{n!} W_{LS}(\omega - \omega_{0-0} - n\omega_0) \qquad (1)$$

where ω_{0-0} is the solution-phase 0−0 transition energy and the prefactors of the line shape function W_{LS} are the familiar Franck−Condon factors. The HR factor λ^2 that best reproduces the relative vibronic intensities in the measured (solvated) PDI spectrum is $\lambda^2 \approx 0.57$.

The PDI_2 complexes show quite different spectra. Although the concentrations of the monomer and dimer complex were

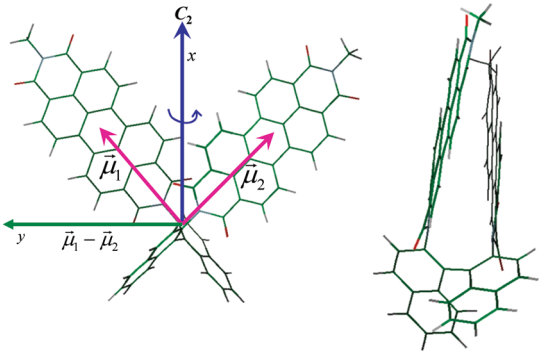

Figure 1. Structure of PDI_2, optimized at the PM3 level, from two side views. The C_2 axis is shown as a blue arrow in the left view, along with the two PDI transition dipoles, $\vec{\mu}_1$ and $\vec{\mu}_2$, shown as magenta arrows, and the $\vec{\mu}_1 - \vec{\mu}_2$ vector, shown as a green arrow. ($\vec{\mu}_1 + \vec{\mu}_2$ coincides with the C_2 axis or x axis). The angle between $\vec{\mu}_1$ and $\vec{\mu}_2$ is approximately $\phi = 86°$.

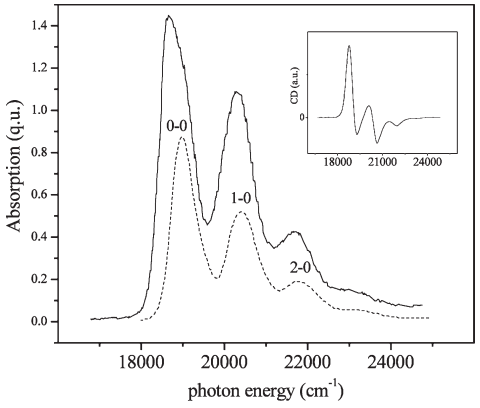

Figure 2. Measured absorption spectra for the PDI monomer (dotted) and the PDI_2 complex of Figure 1 in chloroform from ref 8. Inset: Measured CD spectrum for the right-handed PDI_2 complex.

taken to be equal in Figure 2, the dimer complex is clearly not simply twice the monomer spectrum. First, the relative vibronic intensities are different; for example, the dimer complex would require an effective HR factor of roughly 0.76 to account for the relative intensities of the first two peaks. In addition, there is a clear shoulder on the blue side of the first main absorption peak due to the Davydov splitting caused by the excitonic interactions between the two chromophores.

The CD spectrum, also reproduced from ref 8, is shown in the inset of Figure 2. The spectrum also displays significant vibronic activity and corresponds to the right-handed enantiomer. The vibronic peaks can be crudely described as a series of bisignate peaks and reflect the presence of substantial excitonic coupling between the PDI chromophores.

III. MODEL

In this section, we introduce the Hamiltonian for PDI_2, which treats each PDI molecule as an individual chromophore within a through-space coupled dimer, that is, a Frenkel dimer. Each chromophore is taken to be an electronic two-level system coupled to a symmetric intramolecular vibration of frequency ω_0. The nuclear potentials corresponding to the ground (S_0) and excited (S_1) states are taken to be harmonic, with the S_1 well shifted with respect to the S_0 well, leading to the nuclear relaxation energy $\hbar\lambda^2\omega_0$.

The PDI_2 Hamiltonian employed in this work is the Holstein-like[35] Hamiltonian. For the subspace containing one singlet excitation, H reads

$$H = \omega_0 \sum_{n=1}^{2} b_n^\dagger b_n + \omega_0\lambda \sum_{n=1}^{2} (b_n^\dagger + b_n)|n\rangle\langle n| + J_{12}(|1\rangle\langle 2| + |2\rangle\langle 1|) + D + \omega_{0-0} + \omega_0\lambda^2 \quad (2)$$

where $\hbar = 1$ is taken. $b_n^\dagger$ (b_n) is the creation (destruction) operator corresponding to the symmetric vibration on chromophore n. The pure electronic state, $|n\rangle$, indicates that chromophore n (=1, 2) is electronically excited to the state S_1 while the other chromophore remains in its electronic ground state, S_0. In eq 2, the first term represents the vibrational energy, and the second term represents the local linear exciton−vibrational (EV) coupling. The third term represents the excitonic coupling between the two PDI chromophores. Finally, D denotes the nonresonant interaction between the two chromophores.

The excitonic coupling, J_{12}, between two chromophores can be theoretically well-approximated by the Coulombic interaction between their monomeric transition densities. Although such a calculation would provide accurate interchromophore coupling, less computationally expensive approximations, especially with aggregate systems of large chromophores, are of practical interest. The simplest approximations, such as the point−dipole approximation, where the coupling is based on the interaction of the monomeric transition dipoles, break down for interchromophore distances on the order of the length of the chromophore and lack much of the spatial character of a full transition density. In an effort to capture much of that spatial character while maintaining computational efficiency, we used a method in which Mulliken population analysis (MPA) is applied to the monomeric transition density of the bright $\pi\pi^*$ excited state (S_1) for each PDI. Here, the monomeric transition density is derived from a single-reference excited-state calculation using time-dependent density functional theory (TDDFT), by expanding the excited-state wave function in terms of its single-excitation Slater determinants and their corresponding configuration interaction (CI) coefficients. This has been done recently for carbon nanotubes within the TDDFT regime,[36] although the transition densities from other single-excitation excited-state methods have also been used.[36−39] The MPA analysis of the transition density decomposes the density to point charges, q^t, located at the atomic positions of the chromophore, much as applying MPA to the ground-state density gives partial atomic charges for the ground-state molecule. Within the MPA framework, the q^t values (in atomic units) are calculated as

$$q_P^t = 2 \sum_{b}^{N_P} \sum_{c}^{N} \sum_{j}^{\text{unoccupied}} \sum_{i}^{\text{occupied}} A_{ij} c_i^{Pb} c_j^c S_{Pb,c} \quad (3)$$

where, for an atom P, b is the atomic-orbital (AO) index for that atom; N_P is its number of AOs; c is the AO index for an entire molecular orbital (MO); N is the total number of AOs making up an MO; and A_{ij} is the CI coefficient for the determinant where an electron is excited from occupied MO i to unoccupied MO j, with the total sum of A_{ij} normalized to a value of 1. Furthermore, c_i^{Pb} is the bth AO coefficient centered on atom P of the ith occupied MO; c_j^c is the cth AO coefficient of the jth unoccupied MO; $S_{Pb,c}$ is the overlap between these two AOs; and i and j span the total number of occupied and unoccupied MOs, respectively. The atomic orbital basis set used was Dunning's cc-pVDZ basis.[40] Although it is well-known that atomic charges derived from MPA of the ground-state density can predict inaccurate ground-state dipole moments and are also very sensitive to the AO basis set chosen, q^t derived from MPA do not, in general, have these problems. Indeed, the stability of the method with respect to basis set has been mentioned previously,[36] and in a forthcoming publication, we will demonstrate this comprehensively for a variety of chromophore types in a benchmark theoretical study. In addition, the transition dipole magnitude for PDI is predicted well from MPA-derived q^t values using the TDDFT transition density, at 8.4 D, compared to experiment (8.5 D).

The coupling, J_{12}, between chromophores 1 and 2 appearing in eq 2 can then be efficiently calculated from a simple Coulombic charge−charge interaction between the transition charges on one chromophore with those of the other, such that

$$J_{12} = \sum_i \sum_j \frac{q_i^t q_j^t}{|R_i^{(1)} - R_j^{(2)}|} \quad (4)$$

where i and j are the atom indices corresponding to chromophores 1 and 2, respectively; $\mathbf{R}_i^{(m)}$ is the position of the ith atom on chromophore m; and ε_0 is the vacuum gas permittivity constant. The bichromophore PDI_2 in Figure 1 was optimized at the PM3 level, and then the binaphthalene portion was removed, and reasonable methyl groups were attached to the nitrogens previously attached to the binaphthalene ring carbons, creating two separate *N,N*-dimethyl PDI chromophores with the same PDI atomic positions as in PDI_2. In this manner, we evaluated the coupling (in cm^{-1}) between the two PDI portions to be

$$J_{12} \equiv \langle 1|H|2\rangle = 371 \text{ cm}^{-1} \quad (5)$$

The positive sign of the coupling assumes that the relative phases of the localized wave functions are defined through the relation, $|2\rangle = \hat{C}_2|1\rangle$, where $\hat{C}_2$ represents a 2-fold rotation about the symmetric C_2 axis (see Figure 1).

dx.doi.org/10.1021/jp208794t |J. Phys. Chem. B 2012, 116, 77–86

The Hamiltonian in eq 2 is represented in a one- and two-particle basis set.[41,42] Single-particle excitations, $|n,\tilde{\nu}\rangle$, consist of a vibronically excited chromophore at site n with $\tilde{\nu}$ excited-state quanta in the (shifted) excited-state nuclear potential. The other molecule is electronically and vibrationally unexcited. A vibronic/vibrational pair excitation, denoted $|\, n, \tilde{\nu}; n', \nu'\rangle$ $(n \neq n')$, is a two-particle state because it involves excitations on both molecules. In addition to a vibronic excitation at n, this state includes a vibrational excitation at n' $(\neq n)$ with ν' (≥ 1) quanta in the ground-state potential. For a dimer, there are no three- or higher-particle states. In all calculations that follow, we impose an upper limit of six on the total number of vibrational quanta.

Because of the inherent C_2 symmetry of the dimer of Figure 1, all eigenfunctions are either symmetric (+) or antisymmetric (−) under C_2 rotation. Hence, the αth symmetric or antisymmetric eigenstate of H can be written in the form

$$|\psi_{\pm}^{(\alpha)}\rangle = \sum_{\tilde{\nu}=0,1,2,\ldots} c_{\pm,\tilde{\nu}}^{(\alpha)}(|1,\tilde{\nu}\rangle \pm |2,\tilde{\nu}\rangle) + \sum_{\tilde{\nu}=0,1,2,\ldots}\sum_{\nu'=1,2,\ldots} c_{\pm,\tilde{\nu},\nu'}^{(\alpha)}(|1,\tilde{\nu};2,\nu'\rangle \pm |2,\tilde{\nu};1,\nu'\rangle) \quad (6)$$

where α = 1, 2, ..., in order of increasing state energy. The transition energies of the states $|\psi_{+}^{(\alpha)}\rangle$ and $|\psi_{-}^{(\alpha)}\rangle$ are denoted as $\omega_{+,\alpha}$ and $\omega_{-,\omega}$ respectively.

When vibronic coupling is absent in the bichromophoric complex, there are just two excited states: an antisymmetric exciton shifted by $-J_{12}$ due to intermolecular coupling and a higher-energy symmetric exciton shifted by $+J_{12}$. In the absorption spectrum, the two peaks give rise to the so-called Davydov components. The magnitude of the energetic separation between the components is referred to as the Davydov splitting (DS). In the free exciton limit (no vibronic coupling), the DS is simply $2J_{12}$ (recall $J_{12} > 0$). When vibronic coupling is activated (and $J_{12} \ll \lambda^2\omega_0$), each $n-0$ vibronic peak in the monomer spectrum is split into a lower and upper Davydov component with the splitting approximately equal to

$$\mathrm{DS}_{n-0} \approx 2J_{12}e^{-\lambda^2}\lambda^{2n}/n! \quad (7)$$

as demonstrated in the energy level diagram in Figure 3. The symmetric (upper Davydov) states are polarized in the direction of $\boldsymbol{\mu}_1 + \boldsymbol{\mu}_2$ (defined as the x axis), whereas the antisymmetric (lower Davydov) states are polarized in the direction of $\boldsymbol{\mu}_1 - \boldsymbol{\mu}_2$ (defined as the y axis). Here, $\boldsymbol{\mu}_1$ and $\boldsymbol{\mu}_2$ are the long-axis-polarized $S_0 \rightarrow S_1$ transition dipole moments of molecules 1 and 2, respectively (see Figure 1). Because the molecular dipoles are of equal magnitude, the two polarization directions are orthogonal. In cases where the two PDI molecules are perfectly cofacially overlapping, $\boldsymbol{\mu}_1$ and $\boldsymbol{\mu}_2$ point along a common direction, and the lower Davydov component is forbidden.

IV. ABSORPTION AND CD SPECTRA

The Davydov components are clearly identified by decomposing the unpolarized (dimensionless) absorption spectrum $A(\omega)$ into its components $A_+(\omega)$ and $A_-(\omega)$ along the x and y axes, respectively, as defined in Figure 1

$$A(\omega) = A_+(\omega) + A_-(\omega) \quad (8a)$$

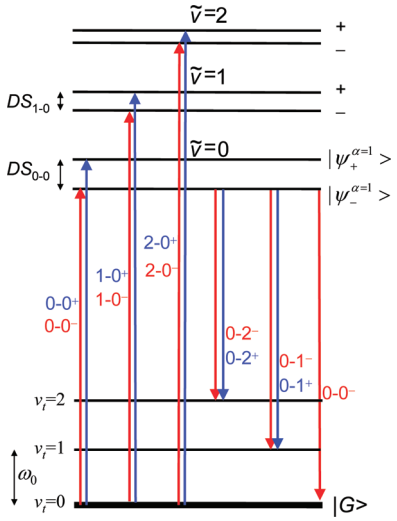

Figure 3. Energy level diagram for PDI_2 in the limit of weak excitonic coupling and low temperature showing absorption transitions (left) and emission transitions (right). Blue (red) transitions are x- (y-) polarized. Energy level ordering is consistent with $J_{12} > 0$. Only ground and excited electronic levels with two or fewer vibrational quanta are shown. Note that the optical gap is not to scale.

with

$$A_{\pm}(\omega) = \frac{1}{{\mu_1}^2}\sum_{\alpha} |\langle G|\hat{\mathbf{M}}_{\pm}|\psi_{\pm}^{(\alpha)}\rangle|^2 W_{LS}(\omega - \omega_{\pm,\alpha}) \quad (8b)$$

Here, $|G\rangle$ is the vibrationless ground state consisting of the product of the pure electronic ground state, $|\, g\rangle \equiv |\, g_1 g_2\rangle$, and the vacuum vibrational state (relative to S_0) and W_{LS} is a symmetric line shape function. $\hat{\mathbf{M}}_+$ and $\hat{\mathbf{M}}_-$ are the symmetry-adapted components of the transition dipole moment (tdm) operator, $\hat{\mathbf{M}} \equiv \hat{\mathbf{M}}_+ + \hat{\mathbf{M}}_-$, with

$$\hat{\mathrm{M}}_{\pm} = \frac{1}{2}(\boldsymbol{\mu}_1 \pm \boldsymbol{\mu}_2)(|g\rangle\langle 1| \pm |g\rangle\langle 2| + h.c.) \quad (9)$$

In eq 9, *h.c.* indicates the Hermitian conjugate.

The CD spectrum is obtained using the expression

$$\mathrm{CD}(\omega) = \sum_{\alpha} R_{+,\alpha} W_{LS}(\omega - \omega_{+,\alpha}) + \sum_{\alpha} R_{-,\alpha} W_{LS}(\omega - \omega_{-,\alpha}) \quad (10)$$

with the rotational strength corresponding to the transition to the state α in the symmetric or antisymmetric manifold given by

$$R_{\pm,\alpha} = \frac{k_l}{2{\mu_1}^2}\left\langle \psi_{\pm}^{(\alpha)}|\hat{\boldsymbol{\mu}}_1|G\right\rangle \times \left\langle G|\hat{\boldsymbol{\mu}}_2|\psi_{\pm}^{(\alpha)}\right\rangle \cdot \mathbf{r}_{12} \quad (11)$$

In eq 11, the tdm operator for the nth chromophore is given by

$$\hat{\boldsymbol{\mu}}_n = \boldsymbol{\mu}_n(|n\rangle\langle g| + |g\rangle\langle n|) \quad n = 1,2 \quad (12)$$

and the separation vector is, $\mathbf{r}_{12} \equiv \mathbf{r}_1 - \mathbf{r}_2$, where $\mathbf{r}_n$ is the center of mass of the nth chromophore. Finally, $k_l = \omega_{0-0}/c$.

dx.doi.org/10.1021/jp208794t |J. Phys. Chem. B 2012, 116, 77–86

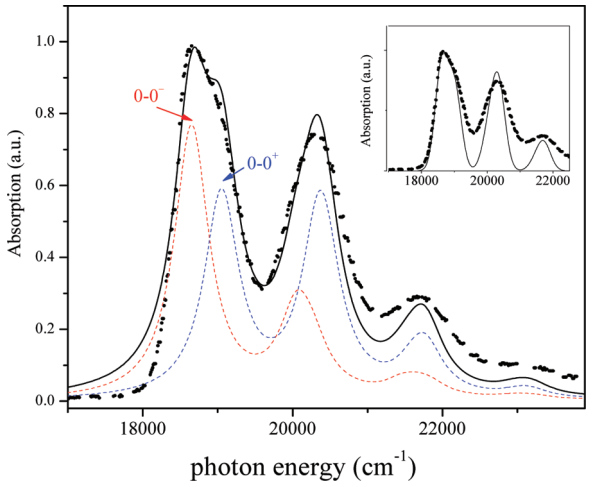

Figure 4. Calculated unpolarized absorption spectrum (black) and components polarized along the x axis (blue) and y axis (red). The measured spectrum from ref 8 is also shown (black dots). Parameters used in the calculation: $J_{12} = 371\ \text{cm}^{-1}$, $\lambda^2 = 0.57$, $\omega_0 = 1400\ \text{cm}^{-1}$ and $\omega_{0-0} + D = 18900\ \text{cm}^{-1}$ ($D = -100\ \text{cm}^{-1}$). The line shape used is Lorentzian with fwhm $=0.4\omega_0$. In the inset, the line shape is Gaussian with full width $(1/e) = 0.4\omega_0$.

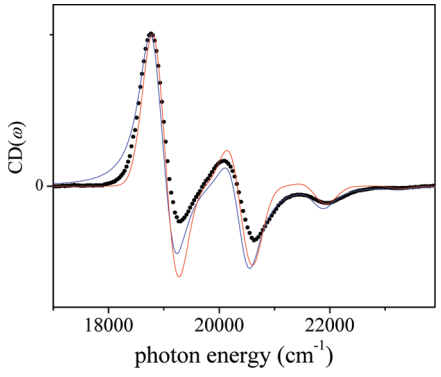

Figure 5. Calculated CD spectrum using the Lorentzian (blue) and Guassian (red) line shapes from Figure 4. Black dots correspond to the measured spectrum from ref 8. The parameters used are the same as in Figure 4.

V. ABSORPTION AND CD: COMPARISON TO EXPERIMENT

Figure 4 shows the measured absorption spectrum for PDI_2 from ref 8 alongside the calculated unpolarized absorption spectrum $A(\omega)$ obtained using the computed coupling ($J_{12} = 371\ \text{cm}^{-1}$) and the HR factor ($\lambda^2 = 0.57$) determined from the monomer solution spectrum in Figure 2. Because $\hbar = 1$, one can view ω as the photon energy and express it in wavenumbers. Figure 5 shows the calculated compared to the measured CD spectrum for the right-handed complex.

In Figure 4, we used a peak-normalized Lorentzian line shape function with a full width at half-maximum of $0.4\omega_0$. In the inset, a Gaussian line shape with a full width $(1/e)$ equal to $0.4\omega_0$ was used.

Overall, the calculated spectrum in Figure 4 does an excellent job in reproducing the relative vibronic peak intensities, as well as the blue shoulder in the main absorption peak. It is clear from the inset that a Gaussian function does a superior job in reproducing the spectral line shape of the main absorption peak, especially the blue shoulder; the line widths of the subsequent peaks are, however, too narrow compared with experiment and are better described using the single Lorentzian. Most likely, the higher-energy sidebands show broadening as a result of the involvement of several closely spaced vibrational modes in the vicinity of the vinyl stretch. Our inclusion of a single vibrational mode is, in fact, an approximation and should be viewed as an effective mode.[43] In a more sophisticated multimode calculation, the first vibrational sideband (second main peak) would be composed of several closely spaced Gaussians, one for each mode. Nevertheless, our single-mode theory with an effective HR factor of 0.57 manages to reproduce the relative vibronic oscillator strengths, as determined by the vibronic peak areas.

Figure 4 also shows the calculated polarized absorption spectra corresponding to light polarized along the x and y axes defined in Figure 1 due to the symmetric and antisymmetric excitons, respectively. Vibronic progressions corresponding to the symmetric (antisymmetric) excitons are labeled as $0{-}0^+$, $1{-}0^+$, $2{-}0^+$, ... ($0{-}0^-$, $1{-}0^-$, $2{-}0^-$, ...), in order of increasing energy, see Figure 3. The DS corresponding to the first main absorption peak was determined to be

$$\text{DS}_{0-0} = \hbar\omega_{+,1} - \hbar\omega_{-,1} = 403\ \text{cm}^{-1}$$

which agrees well with $420\ \text{cm}^{-1}$ predicted from eq 7 using an HR factor of 0.57. The DS values for subsequent peaks are significantly smaller and cannot be discerned from the unpolarized spectrum.

The two polarized line shapes in Figure 4 are quite different; in the x-polarized absorption spectrum due to the symmetric exciton, the ratio of the origin to the first sideband oscillator strengths, $I_A^{(0-0)^+}/I_A^{(1-0)^+}$, is approximately unity, much smaller than the corresponding value of 1.75 measured in the monomer spectrum (see Figure 2). By contrast, the ratio corresponding to the y-polarized spectrum (antisymmetric exciton) is much larger than the monomer value, $I_A^{(0-0)^-}/I_A^{(1-0)^-} \approx 2.48$. In ref 7, it was shown that a readily identifiable spectral signature of ideal J- (H-) aggregates is an increase (decrease) in the ratio of oscillator strengths I_A^{0-0}/I_A^{1-0} upon aggregation. In this regard, the higher energy (x-) polarized component of the dimer spectrum strongly resembles that of an ideal H-aggregate, while the lower energy (y-) polarized component resembles that of an ideal J-aggregate.

An additional indicator of aggregation is the CD spectral line shape shown in Figure 5. The spectra show a series of vibronic bisignate line shapes, a clear signature of vibronic excitons, where the coupling strength is revealed through the magnitude or strength of the CD response. The line shape strongly resembles that displayed by chiral perylene dianhydride aggregates,[44] which are thought to consist of a helical array of chromophores. Figure 5 also shows the spectra calculated using eqs 10 and 11 with a pitch angle of $\phi = 86°$ as determined from PM3 geometry minimization of the bichromophoric complex. The excellent agreement between theory and experiment for Lorentzian and Gaussian line shapes provides strong support for the molecular geometry and our model in general.

VI. ANALYSIS OF THE ABSORPTION SPECTRUM

To more firmly establish the relationship between the absorption spectra of the polarized components of the chiral dimer and those of ideal J- and H-aggregates, we appeal to first-order perturbation theory. A systematic analysis of the effect of excitonic interactions on the vibronic line strengths in various

aggregates was previously considered in refs 4, 6, 7, 45, and 46. A perturbative expression for the oscillator strength ratio of the first two vibronic peaks was derived for H-aggregates with nearest-neighbor coupling only.[45,46] A more general expression, valid for extended interactions and for any aggregate type (J or H) was recently presented in ref 7. For an ideal J- or H-aggregate containing an arbitrary number of molecules and extended couplings, the 0−0/0−1 line strength ratio is determined from

$$\frac{I_A^{0-0}}{I_A^{1-0}} = \frac{1}{\lambda^2}\left[\frac{1 - G(0;\lambda^2)e^{-\lambda^2}\tilde{J}_{k=0}/\omega_0}{1 - G(1;\lambda^2)e^{-\lambda^2}\tilde{J}_{k=0}/\omega_0}\right]^2 \quad |\tilde{J}_{k=0}| \ll \omega_0 \qquad (13)$$

where periodic boundary conditions are assumed. In eq 13, the $k = 0$ interaction sum is given by,

$$\tilde{J}_{k=0} = \sum_s J_{n,n+s}$$

where $s = \pm 1, \pm 2, \ldots$, runs over all neighbors, and the vibrational function $G(v_t;\lambda^2)$ is defined as

$$G(v_t;\lambda^2) \equiv \sum_{\substack{u=0,1,\ldots \\ (u\neq v_t)}} \frac{\lambda^{2u}}{u!(u - v_t)} \qquad v_t = 0, 1, 2, \ldots \qquad (14)$$

Equation 13 reduces to our previously derived expression for polymer H-aggregates[6] when the HR factor is set to unity and only nearest-neighbor couplings are retained. Under the latter condition, $\tilde{J}_{k=0}$ in eq 13 can be replaced by $W/2$, where $W \equiv |\tilde{J}_{k=0} - \tilde{J}_{k=\pi}|$ is the exciton bandwidth. (For nearest-neighbor coupling, $\tilde{J}_{k=0} = 2J_{12}$, and $\tilde{J}_{k=\pi} = -2J_{12}$. Hence, $W = 4J_{12}$, and $\tilde{J}_{k=0} = W/2$.)

Equation 13 applies directly to the cofacial dimer ($\phi = 0°$) when $\tilde{J}_{k=0} = +J_{12}$. For the chiral dimer ($\varphi \neq 0$) with C_2 symmetry, an equation identical to eq 13 holds for the symmetric (antisymmetric) component of the spectrum if $\tilde{J}_{k=0}$ is replaced by $+J_{12}$ ($-J_{12}$). Hence, in the general case of arbitrary ϕ, we obtain

$$\frac{I_A^{(0-0)^\pm}}{I_A^{(1-0)^\pm}} = \frac{1}{\lambda^2}\left[\frac{1 - G(0;\lambda^2)e^{-\lambda^2}J_\pm/\omega_0}{1 - G(1;\lambda^2)e^{-\lambda^2}J_\pm/\omega_0}\right]^2 \quad |J_\pm| \ll \omega_0 \qquad (15)$$

where $J_\pm \equiv \pm J_{12}$. After inserting the values

$$G(\tilde{v}_t = 0;\lambda^2 = 0.57)e^{-0.57} = 0.375$$

and

$$G(\tilde{v}_t = 1;\lambda^2 = 0.57)e^{-0.57} = -0.464$$

into eq 15, we obtain

$$\frac{I_A^{(0-0)^\pm}}{I_A^{(1-0)^\pm}} = \frac{1}{0.57}\left(\frac{1 - 0.375J_\pm/\omega_0}{1 + 0.464J_\pm/\omega_0}\right)^2 \quad |J_\pm| \ll \omega_0 \qquad (16)$$

which gives

$$\frac{I_A^{(0-0)^+}}{I_A^{(1-0)^+}} = 1.13 \quad \text{and} \quad \frac{I_A^{(0-0)^-}}{I_A^{(1-0)^-}} = 2.76$$

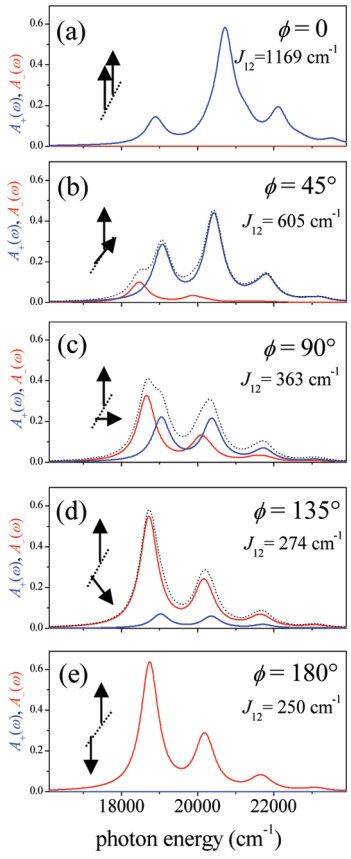

Figure 6. Calculated absorption spectra for PDI_2 complexes with increasing interchromophore angle, ϕ. Black arrows denote the two molecular transition dipole moments, $\boldsymbol{\mu}_1$ and $\boldsymbol{\mu}_2$. The blue (red) spectrum is the *x*- (*y*-) polarized component. (See Figure 1; recall that the *x* axis is the C_2 axis). The dotted curve is the unpolarized sum. The remaining parameters are the same as in Figure 4. Lorentzian line shapes were used with fwhm = $0.4\omega_0$.

for $J_{12} = 371$ cm^{-1}. These values compare favorably with the numerically calculated values of 1.01 and 2.48 for the *x*- and *y*-polarized spectra, respectively.

The nature of the polarized spectra can be further appreciated by varying the interchromophore angle ϕ from 0° to 180° about an axis containing the carbon atoms of each PDI chromophore, which are directly bonded to the naphthalene bridge. (In this calculation, we treat separate PDI molecules; that is, we replace the bridge with *N*-methyls, as described in the Model section.) In this manner, the aggregate evolves from an ideal H-aggregate ($\phi = 0°$, side-by-side) to an ideal J-aggregate ($\phi = 180°$, head-to-tail). The corresponding changes in the absorption spectra are shown in Figure 6. The insets report the calculated couplings, J_{12}, which steadily decrease as ϕ increases but remain positive throughout. We note that a similar analysis of the ϕ-dependent (but unpolarized) absorption spectrum was conducted by Seibt et al.,[26] with spectra qualitatively similar to those in Figure 6.

In the ideal H-aggregate limit ($\phi = 0°$) shown in Figure 6a, only the *x*-polarized spectrum from the symmetric, high-energy excitons are optically allowed. The spectrum shows a substantially weakened $0-0^+$ peak relative to the second vibronic peak ($1-0^+$) due to the strong excitonic coupling, $J_{12} = 1169$ cm^{-1}, resulting from cofacial overlap. The spectrum of Figure 6a, with its depressed 0−0/1−0 peak ratio compared to the monomeric

dx.doi.org/10.1021/jp208794t |J. Phys. Chem. B 2012, 116, 77–86

PDI spectrum (see Figure 2), is very typical of many PDI dimers where the molecules significantly overlap.[10,11,13,17,19] With increasing ϕ value, the ratio $I_A^{(0-0)^+}/I_A^{(1-0)^+}$ increases in response to the decreasing excitonic coupling, characteristic of H-aggregates (see eq 16).

As the angle ϕ increases in Figure 6, one also observes the growth of the *y*-polarized spectrum from the antisymmetric exciton showing clear J-aggregate signatures: The spectrum red shifts with increased excitonic coupling and, in marked contrast to the H-like *x*-polarized spectrum, is dominated by the first vibronic peak ($0-0^-$). As ϕ increases, the *y*-polarized spectrum continues to grow relative to the *x*-polarized spectrum until, when ϕ = 180°, the aggregate becomes an ideal J-aggregate, and only the *y*-polarized spectrum is observed. Moreover, as the exciton coupling decreases in going from Figure 6b to Figure 6e, the ratio $I_A^{(0-0)^-}/I_A^{(1-0)^-}$ also decreases (from approximately 2.8 to 2.2), as expected for ideal J-aggregates (see eq 16).

VII. PHOTOLUMINESCENCE SPECTRUM: THEORY VERSUS EXPERIMENT

In this section, we consider the PL spectrum of the bichromophoric PDI complexes. As for the absorption spectrum, the emission spectrum can be divided into components $S_+(\omega)$ and $S_-(\omega)$ polarized along *x* and *y*, respectively

$$S(\omega) = S_+(\omega) + S_-(\omega) \tag{17}$$

with

$$S_\pm(\omega) = \sum_{\nu_t = 0, 1, 2, \ldots} I_{PL}^{(0-\nu_t)^\pm} W_{LS}(\omega - \omega_{-,\alpha=1} + \nu_t\omega_0) \tag{18}$$

Equation 18 assumes the low-temperature limit where emission takes place from just the lowest exciton, namely, the antisymmetric exciton with $\alpha = 1$. Emission terminates on the ground electronic state with any number of purely vibrational excitations, forming a vibronic progression, as demonstrated in Figure 3. To focus entirely on the impact of aggregation on the oscillator strengths, we have also neglected in eq 18 the cubic frequency dependence found in the Einstein spontaneous emission expression, as well as any influence of a frequency-dependent index of refraction. Hence, we refer to the PL spectrum in eq 18 as a reduced PL spectrum. Equation 18 contains the dimensionless emission line strength for the $0-\nu_t$ transition, given by

$$I_{PL}^{(0-\nu_t)^\pm} \equiv \frac{1}{{\mu_1}^2} \sum_{\nu_1, \nu_2 = 0, 1, 2, \ldots}{}' \left| \left\langle g_1\nu_1, g_2\nu_2 | \hat{\mathbf{M}}_\pm | \psi_-^{(\alpha=1)} \right\rangle \right|^2 \tag{19}$$

where the prime on the summation indicates that the total number of vibrational quanta in the terminal state, $|g_1\nu_1, g_2\nu_2\rangle$, satisfies $\nu_t = \nu_1 + \nu_2$.

Simple group theory shows that the 0−0 transition is always *y*-polarized, because the terminal state, $|g_1\nu_1 = 0, g_2\nu_2 = 0\rangle$, is symmetric under a C_2 rotation. For sideband transitions, however, a mixture of polarizations is possible because the terminal states with one or more vibrational quanta can be symmetric or antisymmetric. Consider, for example, the 0−1 transition. It can terminate on either of two states

$$\frac{1}{\sqrt{2}}(|g_1\nu_1 = 0, g_2\nu_2 = 1\rangle \pm |g_1\nu_1 = 1, g_2\nu_2 = 0\rangle)$$

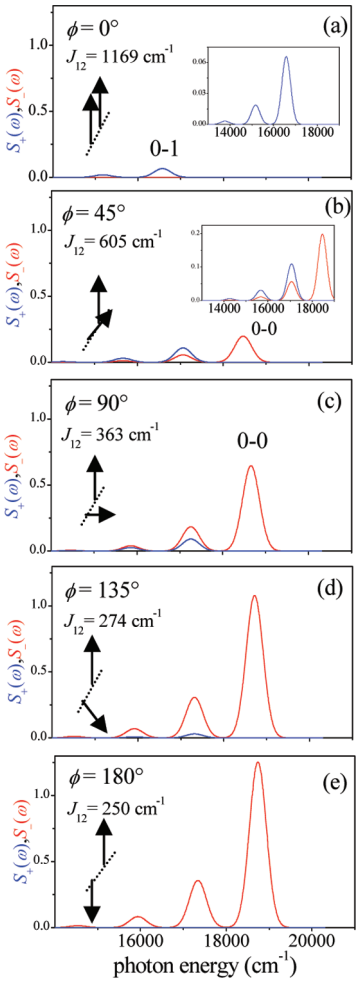

Figure 7. Calculated PL spectra for PDI_2 complexes with increasing interchromophore angle, ϕ. Black arrows denote the two molecular transition dipole moments, $\boldsymbol{\mu}_1$ and $\boldsymbol{\mu}_2$. The blue (red) spectrum is the *x*- (*y*-) polarized component. Insets in (a) and (b) show the magnified spectra. Note the total lack of a 0−0 component in panel a. Gaussian line shapes were used with full width $(1/e) = 0.4\omega_0$. The remaining parameters are the same as in Figure 4.

Group theory then shows that the 0−1 sideband contains a component polarized along *x* when the terminal state in eq 19 is antisymmetric and a component polarized along *y* when the terminal state in eq 19 is symmetric.

Equations 18 and 19 are written in a local basis set with respect to the terminal states. This is possible because we neglect any interactions between ground-state vibrations: they are Einstein phonons with no dispersion. Hence, the $0-\nu_t$ line strength is independent of the basis set chosen for the terminal states.

Figure 7 shows the calculated (reduced) PL spectra as a function of the angle ϕ for the PDI_2 complexes of Figure 6. Several properties are immediately apparent: For an ideal H-aggregate (ϕ = 0°), the two molecular transition dipoles are parallel; hence, there can be no *y*-polarized component because $\boldsymbol{\mu}_1 - \boldsymbol{\mu}_2 = 0$. Equation 19 further shows that the surviving *x*-polarized spectrum cannot support a $0-0^+$ peak because of the symmetry mismatch between the antisymmetric emitting state and the symmetric dipole moment $\boldsymbol{\mu}_+$ (the terminal state, $|G\rangle$, is symmetric in 0−0 emission); see Figure 3. In addition, the sideband progression is very weak because of the strong coupling. All of these properties are consistent with ideal H-aggregates.[7]

dx.doi.org/10.1021/jp208794t |J. Phys. Chem. B 2012, 116, 77−86

As ϕ increases, $\boldsymbol{\mu}_1 - \boldsymbol{\mu}_2$ is no longer zero, allowing the antisymmetric component polarized along y to develop. This y-polarized spectrum is dominated by strong $0-0^-$ emission, which is allowed by symmetry, just as for an ideal J-aggregate. When $\phi = 180°$, an ideal J-aggregate results. Here, $\boldsymbol{\mu}_1 + \boldsymbol{\mu}_2 = 0$, and there can only be y-polarized emission polarized along $\boldsymbol{\mu}_1 - \boldsymbol{\mu}_2$. In this case, the two transition dipole moments in the antisymmetric emitting state, $\boldsymbol{\mu}_1$ and $-\boldsymbol{\mu}_2$, are equal. (In an ideal J-aggregate, this is often described as the $k = 0$ state, where k is the wave vector.)

Hence, in the general case, emission from a chiral dimer complex is both x- and y-polarized. The symmetric (x-polarized) component has the spectral profile of an ideal H-aggregate, and the antisymmetric (y-polarized) component has the spectral profile of an ideal J-aggregate. Note that, if, for some physical reason, the sign of J_{12} becomes negative, then the emitting state would be symmetric, and $\phi = 0°$ (180°) would correspond to an ideal J- (H-) aggregate.

One of the most remarkable features of the y-polarized (J-like) spectrum in Figure 7 is the invariance of the ratio $I_{PL}^{(0-0)^-}/I_{PL}^{(0-1)^-}$ to the angle ϕ and, therefore, to the coupling strength, J_{12}. In Figure 7a–e, the ratio is approximately 3.51, which is equal to $2/\lambda^2$ for $\lambda^2 = 0.57$. We have verified that

$$I_{PL}^{(0-0)^-}/I_{PL}^{(0-1)^-} = 2/\lambda^2 \tag{20}$$

holds for any λ^2, independent of ϕ and J_{12}. In ref 34, we showed that, for aggregates containing two molecules per unit cell (with periodic boundary conditions), the PL ratio is given by

$$I_{PL}^{(0-0)_\rho}/I_{PL}^{(0-1)_\rho} = N/\lambda^2 \tag{21}$$

where N is the total number of chromophores (which must be even for an integral number of unit cells) and ρ indicates the polarization direction of the lower Davydov component. The validity of eq 21 further requires no disorder and $T = 0$ K, so that only the lowest exciton (lower Davydov component) emits. Equation 20 is therefore a special case of eq 21 when $N = 2$.

In Figure 8, we compare our calculated reduced PL spectrum with that derived from the experimental PL spectrum from ref 8. Because the latter was originally reported as a function of wavelength, we first converted to photon energy, which required multiplying the spectrum by the square of the wavelength, λ^2 (because $d\omega$ is proportional to $d\lambda/\lambda^2$) and then divided by the cube of the energy (from the Einstein spontaneous emission expression) to give the reduced PL spectrum. Also shown in Figure 8 are the calculated x- and y-polarized components of the PL spectrum.

The calculated spectra in Figure 8 also contain a Boltzmann average over the emitting states. This is required because the experimental spectra were obtained at 300 K and, at this temperature, there is some thermal excitation of the symmetric state, $|\psi_+^{\alpha=1}\rangle$ (see Figure 3), that can subsequently emit. The most important thermal effect is the nonzero $0-0$ emission observed in the symmetric (x-polarized) spectrum sourced by $|\psi_+^{\alpha=1}\rangle$. This is in accord with the basic property that $0-0$ emission increases with temperature in H-aggregates. In contrast, the $0-0$ component of the y-polarized spectrum is reduced compared to the spectrum at $T = 0$ K, fully consistent with what is expected for ideal J-aggregates.[34,47]

Figure 8 shows that the theory and experiment are generally in good agreement, with the largest disparity involving a significantly larger calculated $0-0$ peak intensity. We expect that the measurements might be susceptible to reabsorption because the optical density of the samples is near unity. There might also be some disorder in the sample, which would make the frequencies of the two chromophores slightly different. Such inhomogeneous broadening will act, similarly to increasing temperature, to reduce the predominant $0-0^-$ peak.[7,34]

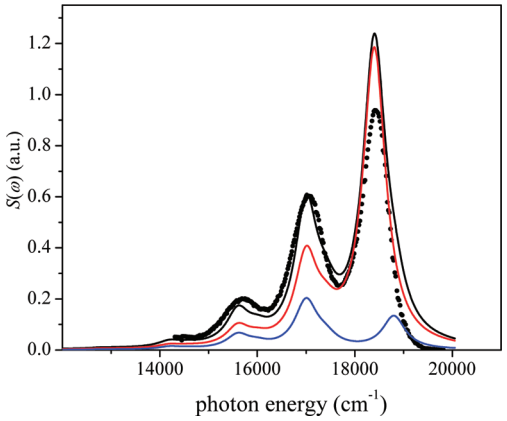

Figure 8. Calculated (reduced) unpolarized PL spectrum (black) and its resolution into x-polarized (blue) and y-polarized (red) components at $T = 300$ K using Lorentzian line shapes. Also shown is the measured spectrum from ref 8 (see text for details). All parameters used in the calculated spectra are identical to those used in Figure 4, except $\omega_{0-0} + D = 18650$ cm^{-1}. The calculated unpolarized spectrum and the measured spectrum were normalized to the $0-1$ peak.

VIII. DISCUSSION AND CONCLUSIONS

Absorption and emission in chiral dimer complexes in which the two chromophores are related by a C_2 symmetry operation can be understood in terms of ideal H- and J-aggregate behavior. When exciton coupling is weak compared to the nuclear relaxation energy, oscillator strength is generally divided between the top and bottom of each vibronic exciton band, giving rise to the two Davydov components as depicted in Figure 3; in the limiting extremes of ideal H- and J-aggregates, where the chromophore transition dipoles are aligned ($\phi = 0°$ and 180°), oscillator strength is concentrated at the top and bottom of each band, respectively, and only a single Davydov component is observed in each vibronic band. Nevertheless, we found that, in the general case for arbitrary ϕ, the absorption component polarized along the direction of the lower Davydov component (y) displays vibronic structure identical to that of an ideal J-aggregate: The oscillator strength ratio, $I_A^{(0-0)^-}/I_A^{(1-0)^-}$, increases as the exciton bandwidth increases (see eq 16). By contrast, the absorption component polarized along the direction of the upper Davydov component (x) is characteristic of an ideal H-aggregate: The oscillator strength ratio, $I_A^{(0-0)^+}/I_A^{(1-0)^+}$, decreases with increasing exciton bandwidth. In addition, the spectral centroid of the upper (lower) Davydov component blue (red) shifts with increasing bandwidth as expected for H- (J-) aggregates. The PL for a dimer complex can be understood in a similar way. Emission originating from the lowest-energy exciton is generally polarized along x and y. Nevertheless, the component polarized in the same direction as the upper (lower) Davydov component strongly resembles ideal H- (J-) aggregate emission with respect to the spectral signatures outlined in ref 7. In the H-like component the $0-0^+$ peak is disallowed by symmetry and the rest of the progression is

depressed with increasing exciton bandwidth. Rising temperature serves to increase the ratio $I_{PL}^{(0-0)^+}/I_{PL}^{(0-1)^+}$ through thermal activation of the upper Davydov component. (Increasing disorder has the same effect.) By contrast, in the J-like component, the ratio $I_{PL}^{(0-0)^-}/I_{PL}^{(0-1)^-}$ is exactly equal to $2/\lambda^2$ (when $T = 0$ K and disorder is absent) independent of the exciton bandwidth. The ratio decreases with increasing temperature (or the addition of disorder) in exact opposition to the H-like spectral component.[34]

For the PDI_2 complexes of ref 8, our single-mode Holstein Hamiltonian, with a through-space excitonic coupling of $J_{12} = 371$ cm^{-1} evaluated quantum mechanically, provides a quantitative account of the absorption, PL, and CD spectral line shapes. The calculated DS of the 0−0 transition is in excellent agreement with the measured DS of approximately 400 cm^{-1}. The success is, in part, due to the large angle of $\phi = 86°$ between the PDI long axes, which prevents significant interchromophore charge transfer, an effect that was not taken into account in the present model. For sandwich-type PDI complexes ($\phi \approx 0$), emission is often dominated by excimers.[13,14] Seibt et al.[27] showed that, in self-assembled PDI sandwich dimers, exciton self-trapping along an intermolecular torsional coordinate is a primary cause of excimer emission.

The dimer complex can be viewed as the basic building block of the herringbone lattice, a common packing motif for many rod-shaped conjugated molecules. In a (two-dimensional) herringbone lattice, the two molecules in a unit cell are usually related through a glide translation or screw rotation, giving rise to the two Davydov components with exciton shift energies $\tilde{J}_{11} \pm \tilde{J}_{12}$.[32,33] Here, $\tilde{J}_{11}$ represents the ($k = 0$) dipole sum involving interactions between equivalent molecules, whereas $\tilde{J}_{12}$ represents the ($k = 0$) dipole sum involving interactions between inequivalent molecules. Hence, the vibronic structure of the polarized absorption and emission spectra of dimer complexes and herringbone aggregates are very similar, provided that the inequivalent sum is dominant ($|\tilde{J}_{12}| > |\tilde{J}_{11}|$). In such aggregates, the two excitonic shifts have opposite signs: The lower Davydov component shifted by $\tilde{J}_{11} - |\tilde{J}_{12}|$ will always resemble ideal J-aggregate absorption while the upper component shifted by $\tilde{J}_{11} + |J_{12}|$ will always resemble ideal H-aggregate absorption. Here, the absorption ratios are simply obtained by inserting the two $k = 0$ exciton energies ($\tilde{J}_{11} \pm \tilde{J}_{12}$) into eq 13.

Oligothiophenes, OTn, with an even number of thiophene rings (n) crystallize in herringbone layers,[48] with dominant inequivalent interactions leading to a very large Davydov splitting of the order of 1 eV.[49,50] For even n, the molecular symmetry is C_{2h}, and the transition dipole moment corresponding to the lowest optical transition is not aligned with the long (inertial) axis, leading to a slight misalignment of the two transition dipoles in the monoclinic unit cell.[51−53] The ac-polarized absorption spectrum is dominated by the blue-shifted H-band, with a much weaker ac-polarized peak near the origin (A_0).[54] By contrast, the b-polarized spectrum is much weaker (because of the nearly parallel transition dipoles) but dominated by the origin vibronic peak as expected for an ideal J-aggregate. (There is, however, significant complexity at higher energies in the b-polarized spectrum introduced by charge-transfer transitions.[55]) Emission contains both components, a b-polarized origin (J-like) followed by ac-polarized sidebands (H-like).[51] Overall, the behavior qualitatively resembles a chiral dimer with a small value of ϕ; see Figures 6 and 7.

A second example is crystalline anthracene. In molecular anthracene, the transition dipole moment (tdm) corresponding to the lowest optical transition is along the short molecular axis. In the crystal phase, the two tdm's in the unit cell form an angle of approximately 60°. Although the exciton shifts from through-space coupling are dominated by a large and negative equivalent lattice sum, the introduction of charge transfer between the two molecules in a unit cell acts as an effective "superexchange" contribution to the inequivalent lattice sum, allowing the latter to dominate.[56] Hence, we expect J- and H-like polarized absorption similar to Figure 6b,c, which is indeed the case:[57] The lower-energy component is polarized along the b axis and is dominated by a 0−0 peak that is about twice as large as the 1−0 peak. By contrast, in the higher-energy ac-polarized component, the 0−0 and 1−0 peaks are of roughly equal intensity. Emission is almost entirely b-polarized and, at early times (following impulsive excitation), strongly resembles a J-aggregate with a 0−0 peak several times larger than the 0−1 peak.[58] Very similar behavior is also observed in tetracene.[59]

Finally, we emphasize the importance of eq 21, which relates the 0−0/0−1 PL oscillator strength ratio to the number of chromophores in a disorder-free linear or herringbone aggregate at $T = 0$ K. In ref 34, we showed that, when disorder is present and/or the temperature is nonzero, eq 21 becomes

$$I_{PL}^{(0-0)_\rho}/I_{PL}^{(0-1)_\rho} \approx N_{coh}/\lambda^2 \tag{22}$$

where N_{coh} is the number of coherently connected molecules in the emitting exciton, which, in an aggregate containing N chromophores, can range between N and unity as disorder (or temperature) is increased. Hence, eq 22 allows a straightforward determination of N_{coh} directly from the PL spectrum. In future works, we will investigate the utility of eq 22 in evaluating the coherence number in PDI J-aggregates that strongly fluoresce with a dominant 0−0 PL peak.[9,10]

AUTHOR INFORMATION

Corresponding Author

*E-mail: spano@temple.edu.

ACKNOWLEDGMENT

We are grateful to F. D. Lewis for valuable discussions on the photophysics of perylene diimides. F.C.S. was supported by the National Science Foundation, Grant DMR 0906464. S.M. was supported by the National Science Foundation, Grant CHE-0911474, and Temple University.

REFERENCES

(1) Hochstrasser, R. M.; Kasha, M. *Photochem. Photobiol.* **1964**, *3*, 317–331.
(2) Kasha, M. *Radiat. Res.* **1963**, *20*, 55–70.
(3) McRae, E. G.; Kasha, M. *J. Chem. Phys.* **1958**, *28*, 721–722.
(4) Spano, F. C. *J. Am. Chem. Soc.* **2009**, *131*, 4267–4278.
(5) Spano, F. C.; Clark, J.; Silva, C.; Friend, R. H. *J. Chem. Phys.* **2009**, *130*, 074904.
(6) Clark, J.; Silva, C.; Friend, R. H.; Spano, F. C. *Phys. Rev. Lett.* **2007**, *98*, 206406.
(7) Spano, F. C. *Acc. Chem. Res.* **2010**, *43*, 429–439.
(8) Langhals, H.; Hofer, A.; Bernhard, S.; Siegel, J. S.; Mayer, P. *J. Org. Chem.* **2011**, *76*, 990–992.
(9) Kaiser, T. E.; Stepanenko, V.; Wurthner, F. *J. Am. Chem. Soc.* **2009**, *131*, 6719–6732.

(10) Ghosh, S.; Li, X.-Q.; Stepanenko, V.; Wurthner, F. *Chem.—Eur. J.* **2008**, *14*, 11343–11357.
(11) Shaller, A. D.; Wang, W.; Gan, H. Y.; Li, A. D. Q. *Angew. Chem., Int. Ed.* **2008**, *47*, 7705–7709.
(12) Langhals, H.; Gold, J. *Liebigs Ann./Rec.* **1997**, 1151–1153.
(13) Giaimo, J. M.; Lockard, J. V.; Sinks, L. E.; Scott, A. M.; Wilson, T. M.; Wasielewski, M. R. *J. Phys. Chem. A* **2008**, *112*, 2322–2330.
(14) Veldman, D.; Chopin, S. M. A.; Meskers, S. C. J.; Groeneveld, M. M.; Williams, R. M.; Janssen, R. A. J. *J. Phys. Chem. A* **2008**, *112*, 5846–5857.
(15) Kawai, T.; Kawamura, K.; Tsumatori, H.; Ishikawa, M.; Naito, M.; Fujiki, M.; Nakashima, T. *ChemPhysChem* **2007**, *8*, 1465–1468.
(16) Tsumatori, H.; Nakashima, T.; Kawai, T. *Org. Lett.* **2011**, *12*, 2362–2365.
(17) Wang, W.; Shaller, A. D.; Li, A. D. Q. *J. Am. Chem. Soc.* **2008**, *130*, 8271–8279.
(18) Zeidan, T. A.; Hariharan, M.; Siegmund, K.; Lewis, F. D. *Photochem. Photobiol. Sci.* **2010**, *9*, 916–922.
(19) Hariharan, M.; Zheng, Y.; Long, H.; Zeidan, T. A.; Schatz, G. C.; Vura-Weis, J.; Wasielewski, M. R.; Zuo, X.; Tiede, D. M.; Lewis, F. D. *J. Am. Chem. Soc.* **2009**, *131*, 5920–5929.
(20) Zheng, Y.; Long, H.; Schatz, G. C.; Lewis, F. D. *Chem. Commun.* **2005**, 4795–4797.
(21) Witkowski, A.; Moffitt, W. *J. Chem. Phys.* **1960**, *33*, 872–875.
(22) Fulton, R. L.; Gouterman, M. *J. Chem. Phys.* **1961**, *35*, 1059.
(23) Fulton, R. L.; Gouterman, M. *J. Chem. Phys.* **1964**, *41*, 2280–2286.
(24) Weigang, O. E. *J. Chem. Phys.* **1965**, *43*, 3609.
(25) Weigang, O. E. *J. Chem. Phys.* **1965**, *43*, 71.
(26) Seibt, J.; Marquetand, P.; Engel, V.; Chen, Z.; Dehm, V.; Wurthner, F. *Chem. Phys.* **2006**, *328*, 354–362.
(27) Fink, R. F.; Seibt, J.; Engel, V.; Renz, M.; Kaupp, M.; Lochbrunner, S.; Zhao, H. M.; Pfister, J.; Wurthner, F.; Engels, B. *J. Am. Chem. Soc.* **2008**, *130*, 12858.
(28) Guthmuller, J.; Zutterman, F.; Champagne, B. *J. Chem. Phys.* **2009**, *131*, 154302.
(29) Gao, F.; Zhao, Y.; Liang, W. *J. Phys. Chem. B* **2011**, *115*, 2699–2708.
(30) Hoffmann, M.; Soos, Z. G. *Phys. Rev. B* **2002**, *66*, 024305.
(31) Heinemeyer, U.; Scholz, R.; Gisslen, L.; Alonso, M. I.; Osso, J. O.; Garriga, M.; Hinderhofer, A.; Kytka, M.; Kowarik, S.; Gerlach, A.; Schreiber, F. *Phys. Rev. B* **2008**, *78*, 085210.
(32) Davydov, A. S. *Theory of Molecular Excitons*; Plenum Press: New York, 1971.
(33) Agranovich, V. M. *Excitations in Organic Solids*; Oxford University Press: New York, 2009.
(34) Spano, F. C.; Yamagata, H. *J. Phys. Chem. B* **2011**, *115*, 5133–5143.
(35) Holstein, T. *Ann. Phys.* **1959**, *8*, 325–342.
(36) Wong, C. Y.; Curutchet, C.; Tretiak, S.; Scholes, G. D. *J. Chem. Phys.* **2009**, *130*, 081104.
(37) Chang, J. C. *J. Chem. Phys.* **1977**, *67*, 3901.
(38) Patwardhan, S.; Sengupta, S.; Wurthner, F.; Siebbeles, L. D. A.; Grozema, F. *J. Phys. Chem. C* **2010**, *114*, 20834–20842.
(39) Li, H.; Malinin, S. V.; Tretiak, S.; Chernyak, V. Y. *J. Chem. Phys.* **2010**, *132*, 124103.
(40) Dunning, T. H. *J. Chem. Phys.* **1989**, *90*, 1007–1023.
(41) Philpott, M. R. *J. Chem. Phys.* **1971**, *55*, 2039–2054.
(42) Spano, F. C. *J. Chem. Phys.* **2002**, *116*, 5877–5891.
(43) Roden, J.; Eisfeld, A.; Dvorak, M.; Bunermann, O.; Stienkemeier, F. *J. Chem. Phys.* **2011**, *134*, 054907.
(44) Zhao, J.-S.; Ruan, Y.-B.; R., Z.; Jiang, Y.-B. *Chem. Sci.* **2011**, *2*, 937–944.
(45) Spano, F. C. *J. Chem. Phys.* **2005**, *122*, 234701.
(46) Spano, F. C. *Chem. Phys.* **2006**, *325*, 22–35.
(47) Yamagata, H.; Spano, F. C. *J. Chem. Phys.* **2011**, *135*, 054906.
(48) Taliani, C.; Gebauer, W., *Handbook of Oligo and Polythiophenes*; Wiley-VCN: Weinheim, Germany, 1999.
(49) Petelenz, P.; Andrzejak, M. *Chem. Phys. Lett.* **2001**, *343*, 139–142.
(50) Sun, X. H.; Zhao, Z.; Spano, F. C.; Beljonne, D.; Cornil, J.; Shuai, Z.; Bredas, J.-L. *Adv. Mater.* **2003**, *15*, 818–821.
(51) Meinardi, F.; Cerminara, M.; Sassella, A.; Borghesi, A.; Spearman, P.; Bongiovanni, G.; Mura, A.; Tubino, R. *Phys. Rev. Lett.* **2002**, *89*, 157403-1–157403-4.
(52) Spano, F. C. *J. Chem. Phys.* **2003**, *118*, 981–994.
(53) Spano, F. C. *Annu. Rev. Phys. Chem.* **2006**, *57*, 217–243.
(54) Muccini, M.; Schneider, M.; Taliani, C.; Sokolowski, M.; Umbach, E.; Beljonne, D.; Cornil, J.; Bredas, J. L. *Phys. Rev. B* **2000**, *62*, 6296–6300.
(55) Stradomska, A.; Kulig, W.; Slawik, M.; Petelenz, P. *J. Chem. Phys.* **2011**, *134*, 224505.
(56) Yamagata, H.; Norton, J.; Hontz, E.; Olivier, Y.; Beljonne, D.; Bredas, J. L.; Silbey, R. J.; Spano, F. C. *J. Chem. Phys.* **2011**, *134*, 204703.
(57) Clark, L. B.; Philpott, M. R. *J. Chem. Phys.* **1970**, *53*, 3790–3801.
(58) Ahn, T. S.; Muller, A. M.; Al-Kaysi, R. O.; Spano, F. C.; Norton, J. E.; Beljonne, D.; Bredas, J. L.; Bardeen, C. J. *J. Chem. Phys.* **2008**, *128*, 054505.
(59) Lim, S.-H.; Bjorklund, T. G.; Spano, F. C.; Bardeen, C. J. *Phys. Rev. Lett.* **2004**, *92*, 107402.